AD-A009 941

AMBIENT ELECTRON DENSITY PROFILES FROM HIGH ALTITUDE NUCLEAR EFFECTS CHEMISTRY CODES

Jane A. Keefer

Mission Research Corporation

Prepared for:

Defense Nuclear Agency

14 February 1975

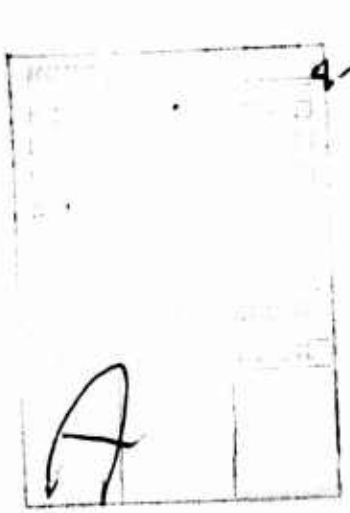

DESTROY THIS REPORT WHEN IT IS NO LONGER NEEDED.
DO NOT RETURN TO SENDER.

UNCLASSIFIED

SECURITY CLASSIFICATION OF THIS PAGE (When Data Entered)

REPORT DOCUMENTATION PAGE		READ INSTRUCTIONS BEFORE COMPLETING FORM
1. REPORT NUMBER DNA 3520T	2. GOVT ACCESSION NO.	3. RECIPIENT'S CATALOG NUMBER AD-A009941
4. TITLE (and Subtitle) AMBIENT ELECTRON DENSITY PROFILES FROM HIGH ALTITUDE NUCLEAR EFFECTS CHEMISTRY CODES		5. TYPE OF REPORT & PERIOD COVERED Topical Report for Period 1 Jan 74-30 Sep 74 6. PERFORMING ORG. REPORT NUMBER MRC-R-145
7. AUTHOR(s) Jane A. Keefer		8. CONTRACT OR GRANT NUMBER(s) DNA 001-74-C-0171
9. PERFORMING ORGANIZATION NAME AND ADDRESS Mission Research Corporation 735 State Street Santa Barbara, California 93101		10. PROGRAM ELEMENT, PROJECT, TASK AREA & WORK UNIT NUMBERS NWED Subtask S99QAXHC065-04
11. CONTROLLING OFFICE NAME AND ADDRESS Director Defense Nuclear Agency Washington, D.C. 20305		12. REPORT DATE 14 February 1975 13. NUMBER OF PAGES<br~~42~~ 37
14. MONITORING AGENCY NAME & ADDRESS(if different from Controlling Office)		15. SECURITY CLASS. (of this report) UNCLASSIFIED 15a. DECLASSIFICATION/DOWNGRADING SCHEDULE

16. DISTRIBUTION STATEMENT (of this Report)

Approved for public release; distribution unlimited.

17. DISTRIBUTION STATEMENT (of the abstract entered in Block 20, if different from Report)

18. SUPPLEMENTARY NOTES

This work sponsored by the Defense Nuclear Agency under Subtask S99QAXHC065-04.

19. KEY WORDS (Continue on reverse side if necessary and identify by block number)

Electron Density Profiles
Atmospheric Chemistry
High Altitude
D, E, and F Regions

20. ABSTRACT (Continue on reverse side if necessary and identify by block number)

Daytime electron density profiles for ambient conditions were computed over the range 60-250 km by adding a solar ionizing source to existing nuclear effects chemistry codes. The computed profiles are in satisfactory agreement with experimental data over most of this altitude range.

DD FORM 1 JAN 73 1473 EDITION OF 1 NOV 65 IS OBSOLETE

UNCLASSIFIED

SECURITY CLASSIFICATION OF THIS PAGE (When Data Entered)

TABLE OF CONTENTS

LIST OF ILLUSTRATIONS

SECTION 1

INTRODUCTION

During recent years, most of the studies of high altitude nuclear bursts have emphasized the effect of the nuclear environment on radar and optical components of weapon systems. Chemistry calculations done as a part of these studies generally assumed a substantial initial disturbance of ambient conditions. It was also generally assumed that the nuclear effects were "over" when the electron density had decayed to approximately 10^6 cm^{-3}. Natural ionization sources which are negligible in comparison with the nuclear sources were not considered.

There is now interest in extending our current capability to compute high altitude nuclear effects to include results that can be used in communication system studies. One of the many questions that needs to be addressed concerns the adequacy of the deionization chemistry calculations. Whereas it is usually assumed that radars would operate satisfactorily in a non-nuclear environment, it is well-known that communication links over a large part of the frequency spectrum can be substantially enhanced or degraded by naturally occurring variations in ionospheric conditions. We therefore need to verify that our calculations of the ionization and deionization that occur following a nuclear burst limit correctly to the ambient electron and ion density in the absence of a nuclear source. This in turn implies that natural ionization sources can no longer be ignored.

This report describes our efforts to incorporate natural ionization sources into the chemistry codes that are used to compute the deionization

following a nuclear burst. We then compute the density of electrons and other species of interest in an ambient atmosphere and compare the results with observations.

SECTION 2

NATURAL IONIZATION SOURCES

DAYTIME SOURCES

The primary ion source in the daytime ambient ionosphere is solar radiation in the ultraviolet, extreme ultraviolet and x-ray regions of the spectrum. Molecular oxygen can be ionized by radiation with wavelengths less than 1028 Å, while the molecular nitrogen ionization threshold occurs at 796 Å. The atomic oxygen and nitrogen thresholds are at 910 Å and 853 Å respectively. Since atomic nitrogen is a very minor species at all altitudes, its photoionization can be safely neglected under ambient conditions and none of the calculations reported here include nitrogen atom photoionization

Another minor species, NO, cannot be neglected as its ionization threshold occurs at 1338 Å and a strong peak in the solar flux associated with hydrogen Lyman-α (H Ly-α) emission occurs at 1215 Å. This H Ly-α radiation is not strongly absorbed by the major atmospheric species and penetrates to lower altitudes than the radiation that ionizes N_2, O_2, and O. In the D-region NO^+ is the primary ion produced by absorption of solar radiation. A discussion of ionization produced at lower altitudes by solar radiation has been given by Bourdreau, et al[1].

The calculation of a solar photoionization rate constant at an altitude, z requires a knowledge of

1. The solar flux at the top of the atmosphere,

2. absorption and ionization cross-sections for the important atmospheric species,

3. densities of the atmospheric species along the absorption path of the solar ray from the topside down to the altitude z.

Such a calculated ionization rate constant will thus reflect, in varying degrees, the level of solar activity which in turn is linked to atmospheric variations in temperature, and density associated with latitude, season, etc.

Detailed topside measurements[2] of the solar spectrum are now available from satellite data, and tabulations of cross-sections and standard atmospheric density profiles can be found in a variety of sources[3,5].

Several computations of solar photoionization rate constants have also been published[4-6]. For the work reported here, we have adopted the set of rate constants given by Keneshea, et al., in Chapter 13 of Reference 5 for N_2, O_2, O and NO as function of altitude and solar zenith angle. These rate constants represent conditions of low solar activity and correspond to a latitude of 30°. Other sets of rate constants appropriate to different conditions could easily be added by expanding the tabular input to the chemistry codes.

Cosmic rays penetrate deeply into the atmosphere causing ionization proportional to the atmospheric density. Thus, above 60-70 km, cosmic rays as a daytime ion source can generally be ignored. Furthermore, the intensity of the cosmic rays decreases with increasing solar activity and decreasing latitude. The existing D-region chemistry code contains a background cosmic ray source[7] and this has been retained. The E and F-region codes do not contain such a source and none was added.

NIGHTTIME SOURCES

In the E and F_1 regions nighttime ionization levels can be several orders of magnitude below daytime levels. Such levels cannot be explained by simply removing the daytime source. Swider's[8] study of nighttime ionospheric processes indicates that some source is required to maintain nighttime E region levels and he suggested that possible sources might be scattered hydrogen Ly-α and Ly-β radiation. Recent rocket probes into the upper atmosphere have confirmed the existence of H Ly-α and H Ly-β nightglow as well as nightglow due to He(504 Å) and HE^+(389 Å) lines[9]. The resulting data indicate that there is sufficient flux of scattered radiation to account for the observed maintenance of the nighttime ionosphere[10].

Following Keneshea, et al.[11], we have attempted to simulate a nighttime source in the E and F regions by reducing daytime photoionization rate constants in such a way as to roughly reflect observed nighttime fluxes.

D-region ionizing sources at night are primarily cosmic rays. Other possible sources at night are the diffuse x-ray background, galactic sources of x-rays[12] and precipitating energetic electrons[13]. Scattered H Ly-α may also play a role[12]. Other than cosmic rays, none of these sources has been included in the D-region code at present, and no nighttime D-region calculations were done.

OTHER SOURCES

Other possible natural ionization sources include energetic electron showers and proton and α-particle bombardments. These sources are generally more important at high latitudes and are often associated with disturbed ion levels such as are observed in auroral and other related phenomena. At present no provision for these types of sources has been made in our nuclear effects chemistry codes. Chemistry codes oriented

towards the study of auroral data have been developed at MRC in support of the ICECAP program[14]. Presumably some of the techniques and methods used in these studies can be applied to our existing codes should the inclusion of natural particle bombardment sources be required in future work.

SECTION 3

CHEMISTRY CODES

THE D-REGION (60-100 km)

A comprehensive code, DCHEM, containing more than 40 species and several hundred reactions has been developed by Scheibe[15]. Included in these reactions are photodissociation and detachment processes. Additionally the code normally expects as input some initial high level ionization source. For the calculations reported here, this source has been set to zero. The background cosmic ray source is retained in its present form of $p = \rho \times 10^{-17}$ ion pairs/cm^{3}sec, where p is the production rate and ρ is the density. The solar photoionization rate constants of Reference 5 were added to the program.

THE E AND F REGIONS (100-300 km)

Two chemistry codes are available for these altitudes and they reflect different levels of sophistication and speed. SDCCHEM is a relatively simple code containing 12 reactions and 8 species, N_2, O_2, NO, N, O, N^+, O^+ and X_2^+, which represents the sum of the molecular ions, NO^+, O_2^+ and N_2^+. A full description of this code is contained in Reference 16. The second code, RK3, contains 15 species including excited $N(^2D)$ and $O^+(^2D)$ and it has about 50 reactions. Further details on this code are given in Appendix A.

Each of these codes contains provisions for instantaneous high level ionizing sources. These were set to zero for all the ambient calculations

reported here and the photoionization rate constants of Reference 5 were added.

INITIAL AND FINAL DENSITIES

The DCHEM code was run with ambient temperature and density profiles, appropriate to the equilibrium daytime D-region composition and to the various photo-chemical rate constants contained in the program. Thus, initial profiles for CO_2, H_2O, O, O_3, NO_2, NO, and $O_2(^1\Delta)$ were included in addition to the major species densities.

Both E and F region codes were run with the same temperature and density profiles used to compute the solar photoionization rate constants[5]. The inclusion of an initial NO profile was found to be important in attaining equilibrium. This profile is still subject to a great deal of uncertainty[17].

Once the initial densities and temperatures were specified, each code was allowed to run out to about 10^4 seconds. Equilibrium with respect to ionization levels was taken to be reached whenever the electron density remained at a steady value. At most altitudes this was reached between 5×10^2 and 5×10^3 seconds. In some cases no steady value was attained. This was true for the D-region results at 60 and 65 km and also for some of the higher altitude F-region calculations.

The electron density profiles reported here are the equilibrium values as defined above. If no equilibrium was reached, the maximum values are given except for the 60 and 65 km results. For these two altitudes the computed electron density begins to oscillate at late times. Therefore, the values reported for these two altitudes are the electron densities computed at 10^3 seconds, the time at which the D-region code indicates that equilibrium is first reached with respect to the electron density.

None of the electron densities reported here is expected to differ by more than a factor of two or three from the true equilibrium value the codes would predict if running time had been extended. Experimental measurements can easily differ by more than this. The experimental profiles chosen for comparison were selected to match the theoretical conditions as closely as possible with respect to solar activity (low), solar zenith angle (χ=30, 60 and 75 degrees) and latitude (30 degrees).

SECTION 4

RESULTS AND DISCUSSION

THE DAYTIME D-REGION

Reported measurements of D-region electron density profiles show variations of as much as an order of magnitude at a given altitude[18]. These variations reflect different levels of solar activity, season, latitude, etc., as well as different experimental techniques. As the altitude decreases, experimental difficulties in detecting the lower electron densities tend to increase.

Two daytime D-region calculations were done using the DCHEM code. One is for a solar zenith angle of 60° and the other is for 30°. The calculated electron densities are compared with experimental profiles in Figures 1 and 2. As expected the computed electron densities are somewhat larger when χ=30° than when χ=60°.

Figure 1 shows the 60° results. Two experimental profiles are given for comparison. The Mechtly and Bowhill[19] data are based on five rocket probes launched from Wallops Island, Virginia (latitude 38°N) during quiet sun years at χ=60°. Mitra and Chakrabarty's[18] profile is a composite of a large number of mid-latitude, low solar-activity, $\chi \cong 60°$ experiments. Thus, the experimental conditions match the assumed theoretical conditions fairly closely. The χ=30° profiles in Figure 2 are less well matched, since this zenith angle will be attained only for a limited time during the year at mid-latitudes. The experimental profile[18] in Figure 2 represents low

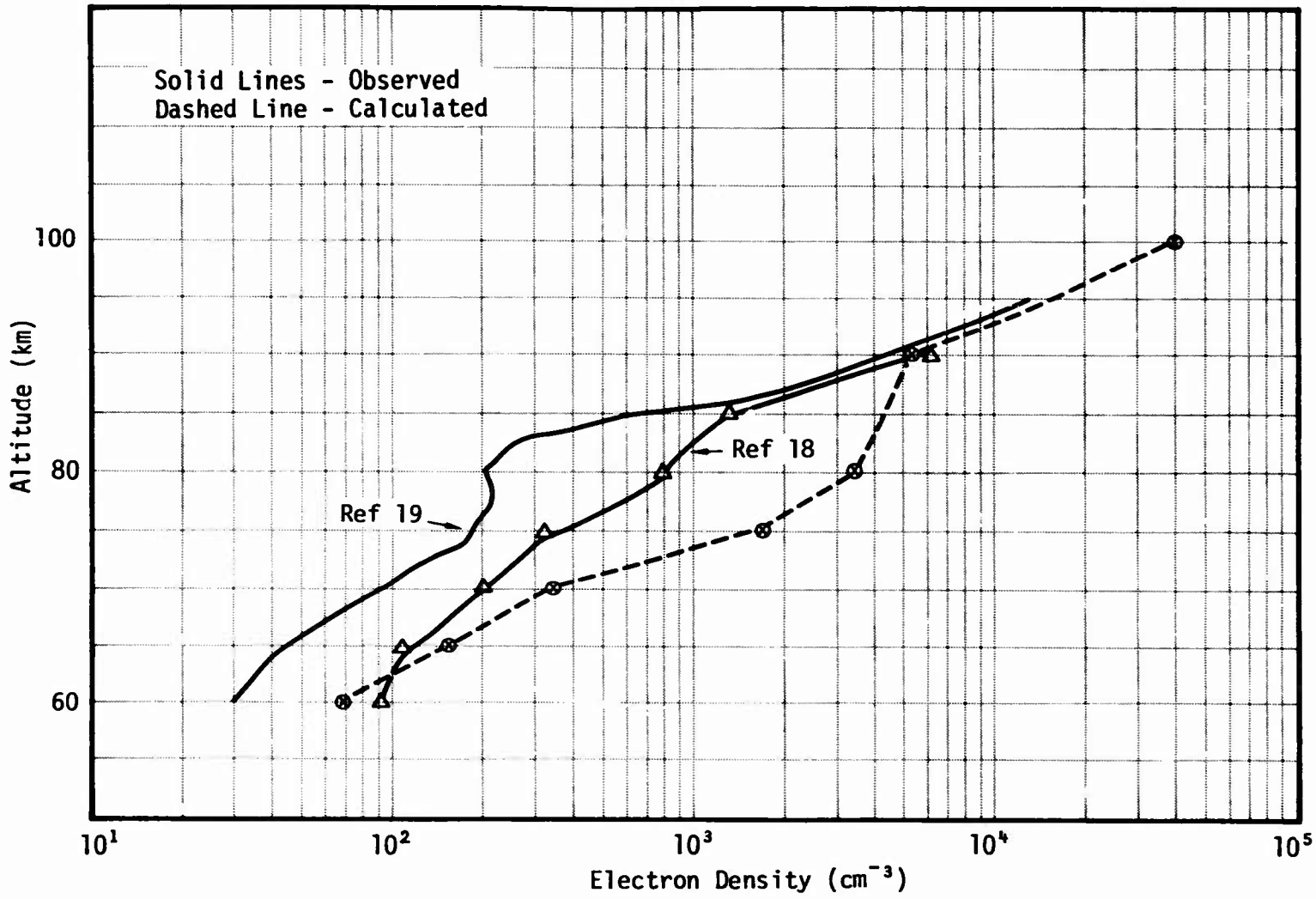

Figure 1. Comparison of Computed and Observed D-Region Electron Density Profiles for $\chi = 60°$.

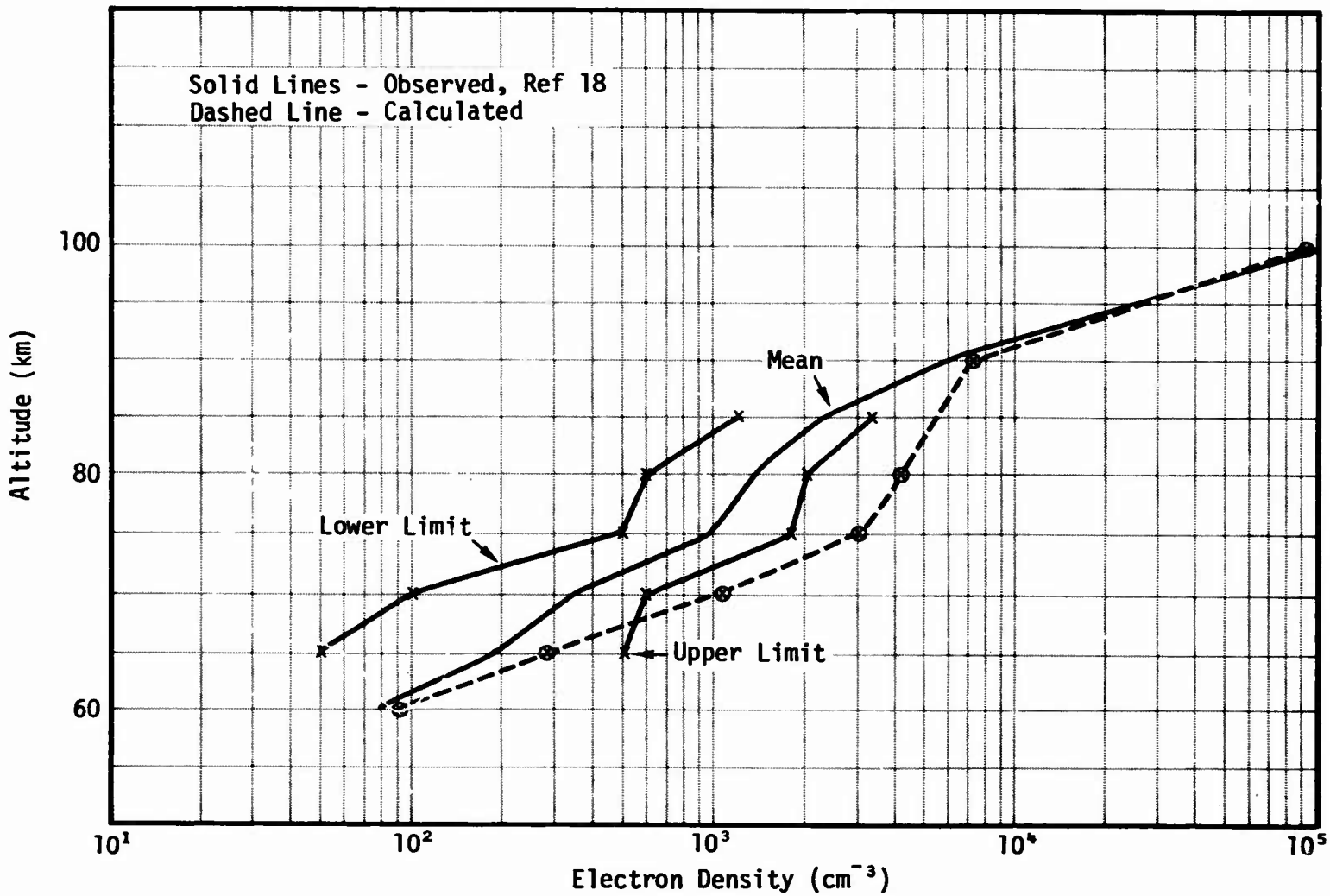

Figure 2. Comparison of Computed and Observed D-Region Electron Density Profiles for $\chi = 30°$.

latitude and medium solar activity for $\chi \cong 30°$. The comparable low-solar-activity, mid-latitude, 30° profile would, perhaps, exhibit somewhat reduced electron densities above 65 km and enhanced densities below this altitude[19].

The overall agreement between both computed and measured profiles is satisfactory, considering the variety of factors which can affect measured electron densities. Mechtly and Bowhill[19] indicate that their χ=60° data is accurate to about 10% at 90-95 km, but below these altitudes, the measurements are subject to increasing uncertainties and error factors as large as two or three may occur around 50-60 km.

The largest discrepancies between theory and experiment are in the 75-85 km region. In this region detachment of O^- and O_2^- occurs either by collisional association with O or by photodetachment. Banks[4] has suggested that the chemical process involving O^- and O_2^- are more efficient than photodetachment in the D-region and the calculated DCHEM destruction rates do, in fact, exhibit this behavior. An excess of atomic oxygen can thus increase the computed electron density. DCHEM consistently computed late-time atomic oxygen profiles that are higher than the initial concentrations and it has done so in the past starting from more disturbed conditions[20].

The most important source of O and O_3 is the photodissociation of O_2 (the resulting O atoms react with O_2 to produce the O_3). The rate constants of most photodetachment processes occurring in the D-region are not strong functions of the solar zenith angle, since significant absorption of dissociating radiation does not occur in or above the D-region. The statement does not apply, however, to the O_2 dissociation. Owing to the large density of O_2, substantial absorption of the dissociating radiation does occur both in and above the D-region. For example at 80 km, the photodissociation rate for χ=60° is computed to be about half of χ=0° (overhead sun) value[21]. In DCHEM, all photodissociation rates are for χ=0°. A

decrease in the O_2 photodissociation rate would decrease atomic oxygen desnity and the associative detachment rates for O_2^- and O^-. However, our χ=30° calculation also tends to overestimate the late-time atomic oxygen profile, so that the inconsistencies cannot be resolved solely on this basis, since the χ=30° photodissociation rate constant is essentially the same as the overhead sun value.

The overestimation of the atomic oxygen may also be due to the lack of transport effects in DCHEM. Theoretical studies by Colgrave, et al.[22] have indicated that observed oxygen profiles in the ambient D-region can be explained only by inclusion of transport effects. Similar conclusions were reached by Strobel, et al.[23], for NO. A general discussion of how dynamic processes can affect the ionization balance in the D-region can be found in Reference 24.

Most likely no one factor can be isolated to account for the apparent overestimation of the electron density by DCHEM in the middle D-region. We have, so far, focused on one possible source of "extra" electrons - the atomic oxygen profile. Another factor is the uncertainty in the nitric oxide profile. A lowering of the NO profile and hence a lowering of the source of the primary NO^+ ions and electrons by a factor of two can easily be justified[25].

Still another factor is the question of ion clustering. Measurements made in the quiescent upper D-region indicate that both the positive and negative ions are, to a large extent, hydrated; i.e., they have formed clusters with water molecules[25-27]. The DCHEM code does not have negative ion hydrates and since these are probably less easily detached by O and $O_2(^1\Delta)$ the DCHEM code will tend to overestimate electron detachment. DCHEM does contain positive ion clustering but the ions it predicts as dominant are not those which are observed. The explanation for this is not yet known. Those that are observed are more heavily hydrated and have larger coefficients

of dissociative recombination with electrons. Thus the DCHEM code underestimates electron recombination.

All of these factors probably combine to yield the higher than observed electron densities reported here.

THE DAYTIME E AND F_1 REGIONS

Daytime electron density profiles computed with solar photoionization rate constants corresponding to zenith angles of 30, 60 and 75° are shown in Figures 3, 4, and 5. The experimental densities at χ=40° and 60° are composite mid-latitude, low activity profiles obtained from a large number of observations[28]. The χ=75° results are compared with rocket data measured one hour after sunrise at Wallops Island in September 1965, a year of low solar activity[29]. All six calculations reproduce the experimental profiles quite well down to 90 km.

As the figures show, the computed SDCCHEM electron densities are always lower than those obtained from RK3. In the E and F_1 regions, electrons are lost mainly through dissociative recombination of NO^+ and O_2^+. SDCCHEM lumps these two processes together with N_2^+ recombination and the rate constant for all three recombination is controlled by the fastest processes, which is the NO^+ dissociative recombination. Hence SDCCHEM tends to recombine electrons more quickly than RK3, which considers each process separately.

Figure 6 compares the calculated O^+ and molecular ion profiles ($X_2^+ = NO^+ + O_2^+ + N_2^+$) at χ=60° with Johnson's composite daytime profile for low solar activity[30]. The computed profiles for O^+ and X_2^+ reproduce the relative behavior of the corresponding experimental densities rather nicely. Johnson's profiles also include N_2^+ which is not shown here. This ion tends to remain about an order of magnitude less than the major X_2^+ ions.

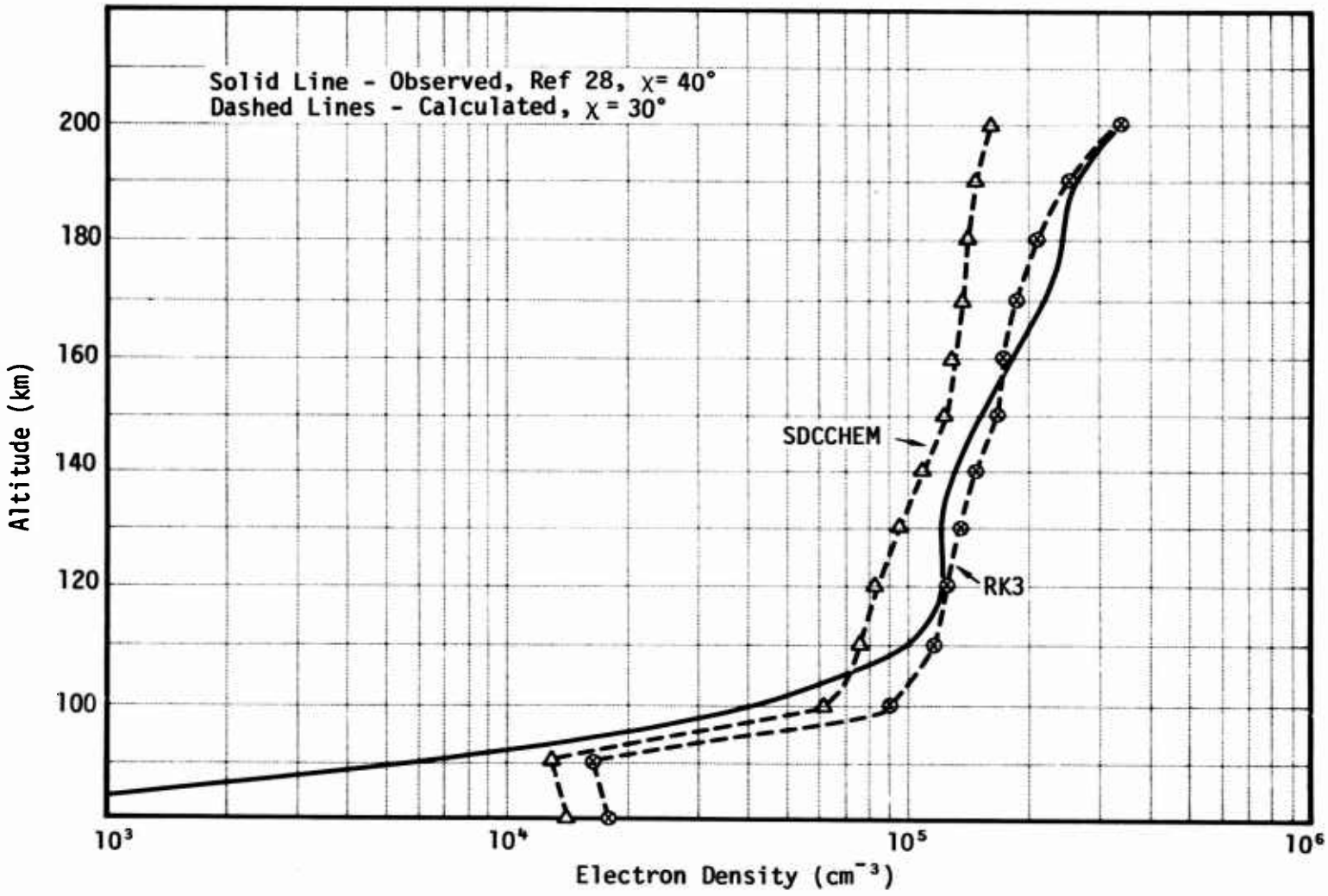

Figure 3. Comparison of Computed and Observed E- and F_1-Region Electron Density Profiles for Small Solar Zenith Angle.

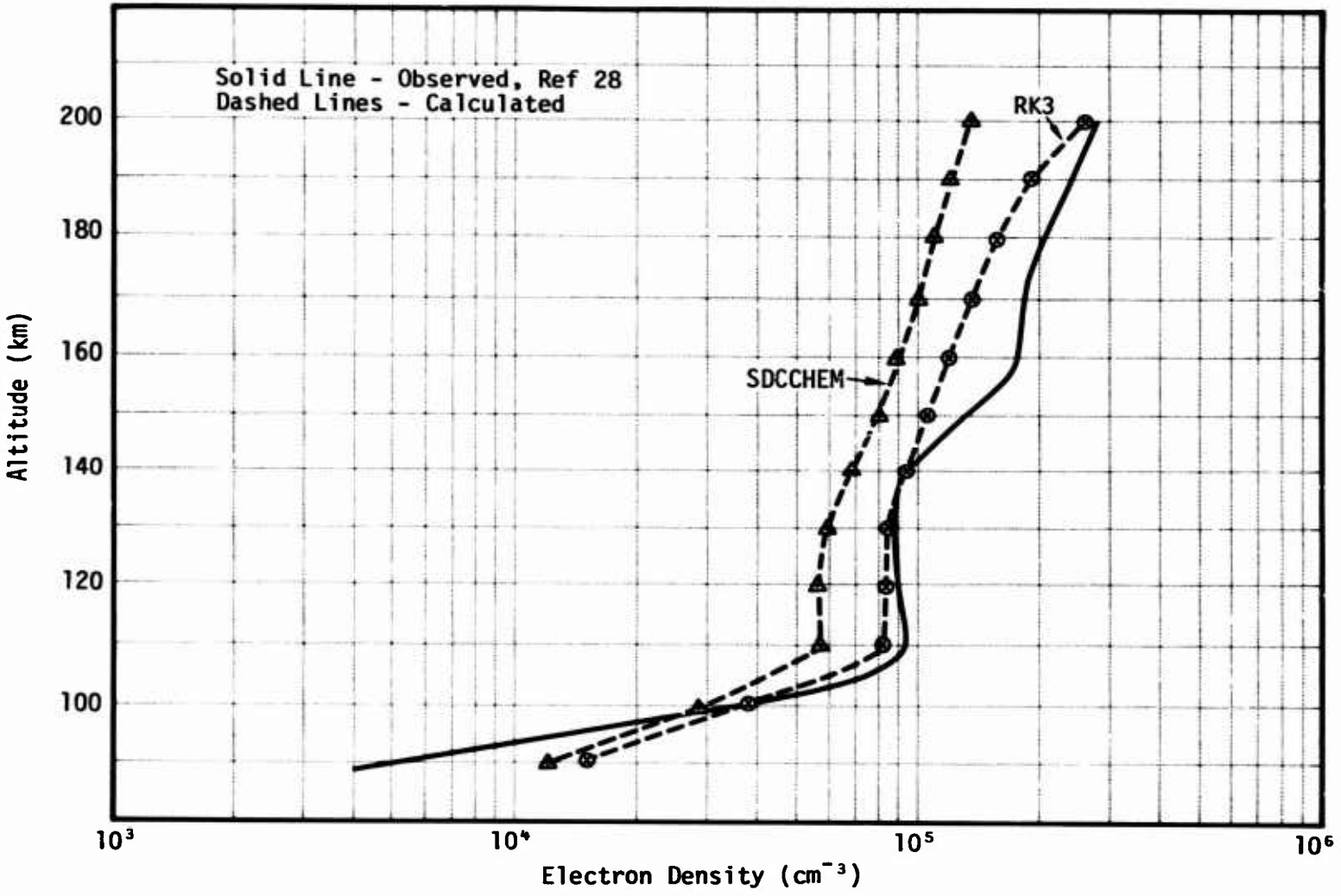

Figure 4. Comparison of Computed and Observed E- and F_1-Region Electron Density Profiles for $\chi = 60°$.

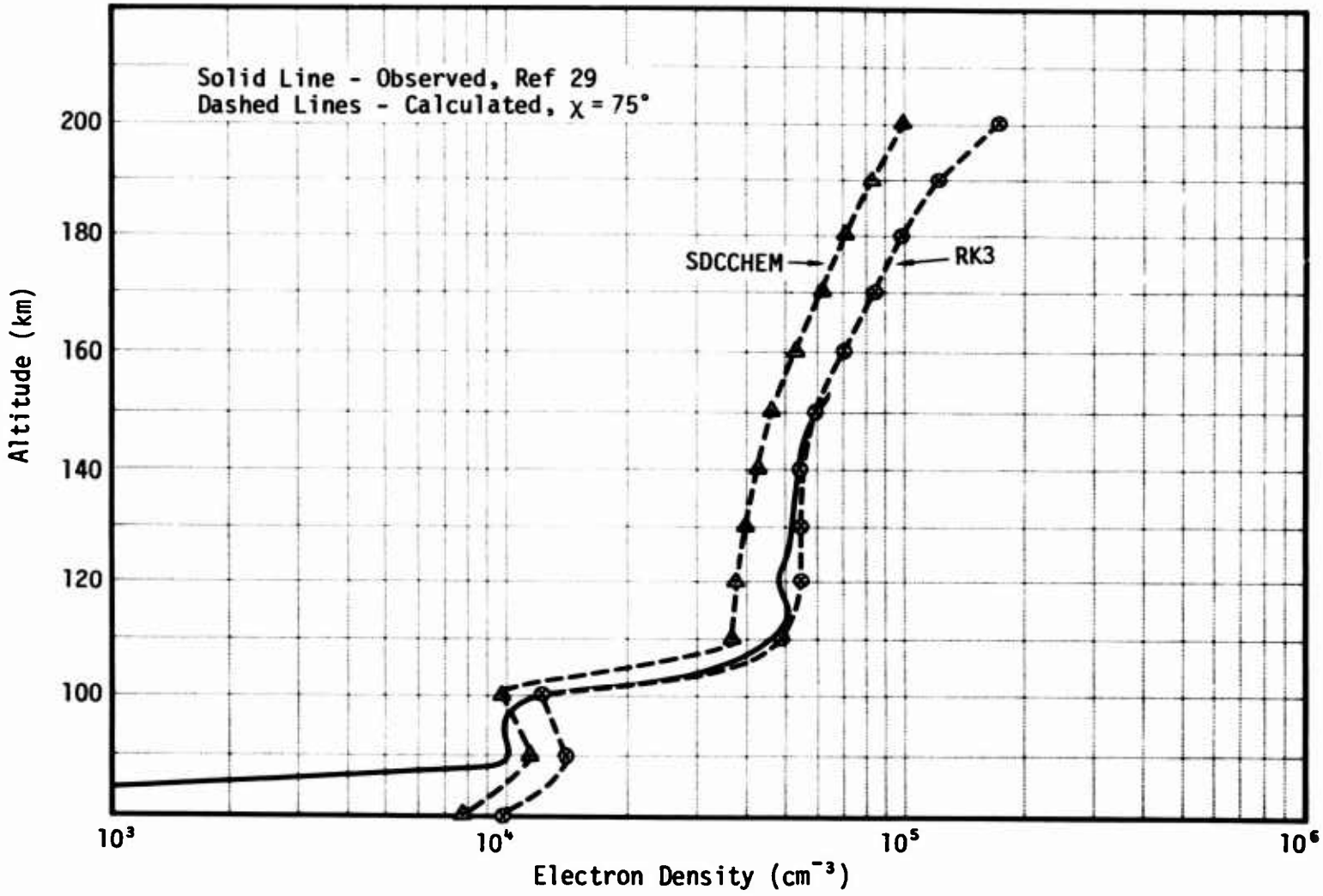

Figure 5. Comparison of Computed and Observed E- and F_1-Region Electron Density Profiles for Large Solar Zenith Angle.

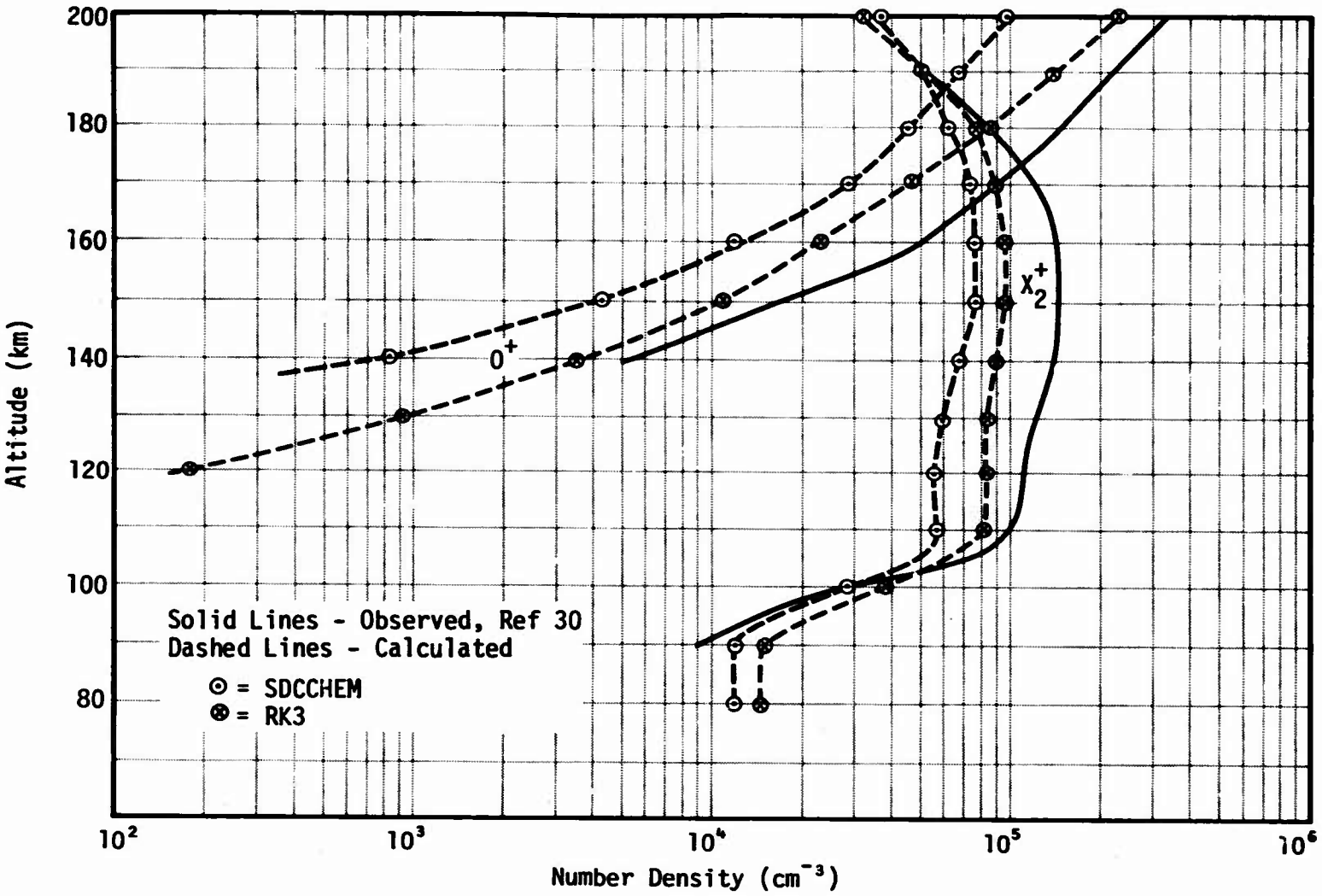

Figure 6. Comparison of Computed and Observed E- and F_1-Region Ion Densities for $\chi = 60°$; X_2^+ Equals the Sum of the Molecular Ions, N_2^+, O_2^+ and NO^+.

RK3 predicted N_2^+ levels are roughly consistent with the observed N_2^+ profile. The ion data in Johnson's composite profile is normalized to different electron density profiles below and above 130 km, and the maximum deviation introduced by this use of different profiles is estimated by Johnson to be no more than 25%. The RK3 results are within 25% of the experimental densities at most altitudes, although they are consistently lower throughout the E and F regions. It is not easy to determine whether this reflects some inconsistency in the chemistry codes or simply a "normal" variation of the experimental profiles. RK3 late-time NO densities are below the initial NO profile. This implies that either the RK3 loss rate for NO is too large or that the NO profile of Reference 6 is too high for the conditions under study. Since the NO profile is still subject to considerable controversy[17], it seems impossible at this time to attribute the depressed late-time NO levels in RK3 solely to shortcomings in the theoretical model.

THE NIGHTTIME E AND F_1 REGIONS

Figure 7 shows a nighttime electron density profile computed by RK3 using a source of hydrogen Ly-α set to 2% of its daytime $\chi=30°$ values. This corresponds to a flux of H Ly-α radiation of about 6×10^9 photons/cm^{2}sec above 100 km as compared to reported values of $4\text{-}6\times10^9$ photons/cm^{2}sec.[4] The experimental profiles[31] are smoothed curves obtained from ionograms at Boulder, Colorado in 1958, a year of intermediate solar activity.

The agreement between theory and experiment is not as satisfactory as the daytime results. The H Ly-α produces NO^+, but no other positive ion, which is consistent with observations[32] that NO^+ is the dominant ion. However, nighttime NO^+/O_2^+ ratios tend to remain constant at around 0.1 which implies that some source is producing O_2^+ [10]. Scattered H Ly-β and HE II (304 Å) and He I (584 Å) fluxes of between 1 and 10×10^6 photons/cm^{2}sec have been reported[9]. In order to reduce the daytime O_2 photoionization rate

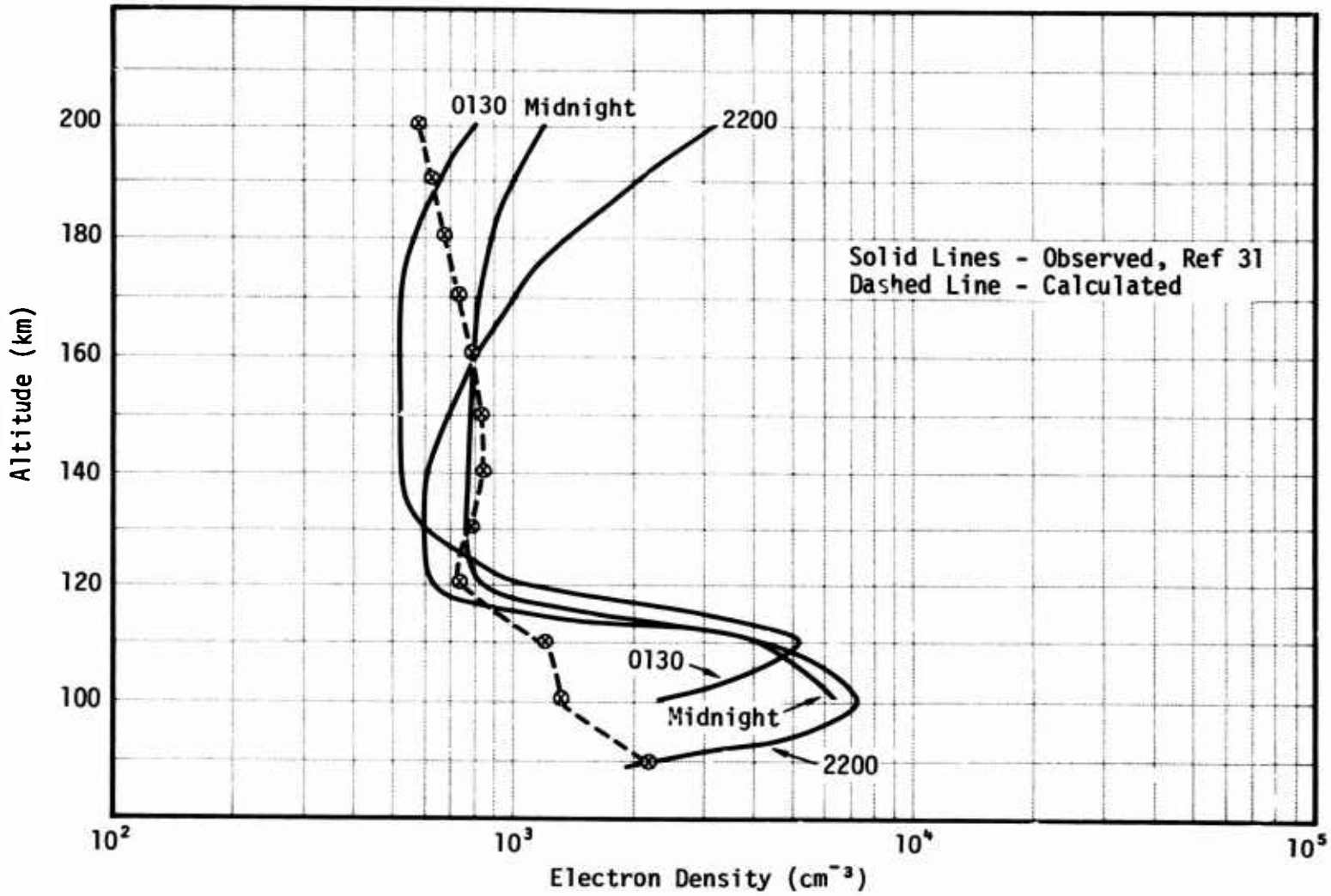

Figure 7. Comparison of Computed and Observed Nighttime E- and F_1-Region Electron Density Profiles.

constant, an estimate is needed of the percentage these particular lines contribute to the total solar spectrum flux. All of these lines are fairly intense compared to the solar continuum and a very rough guess based on the flux tabulations of Banks[4] would be that they represent around 1/10 of the total number of photons below the O_2 ionization threshold. The nighttime fluxes of these lines are at least 5×10^3 less than daytime levels, so that a reduction factor of about 5×10^4 or 0.05% might be appropriate and an order of magnitude variation in this factor could easily be possible. A calculation using 0.05% of the daytime O_2 photoionization rate constant and 1% of the NO rate constant tended to overestimate the nighttime electron density as well as the NO^+/O_2^+ ratio. Since both experimental[33] and theoretical[34] evidence is now beginning to indicate that nighttime ion transport effects in both the E and F regions may be comparable to chemical production and loss rates, we have not attempted at this time to model the nighttime ionosphere in a more detailed fashion.

Finally, it should be noted that the nighttime electron densities computed by SDCCHEM differed from the comparable RK3 values in the same way that the daytime levels did; i.e., they were slightly less than the RK3 values at all altitudes and presumably for the same reasons.

THE DAYTIME F_2 REGION

Figure 8 compares the electron density computed by RK3 with $\chi=30°$ to Johnson's composite profile for low solar activity[30]. The computed values never reached equilibrium above 220 km, an indication, perhaps, that chemical time constants are becoming comparable to ion diffusion times above this altitude.

Diffusion in the upper atmosphere may occur in response to a variety of external forces such as gravity, pressure gradients, neutral atmospheric winds and electric and magnetic fields. The interaction of the

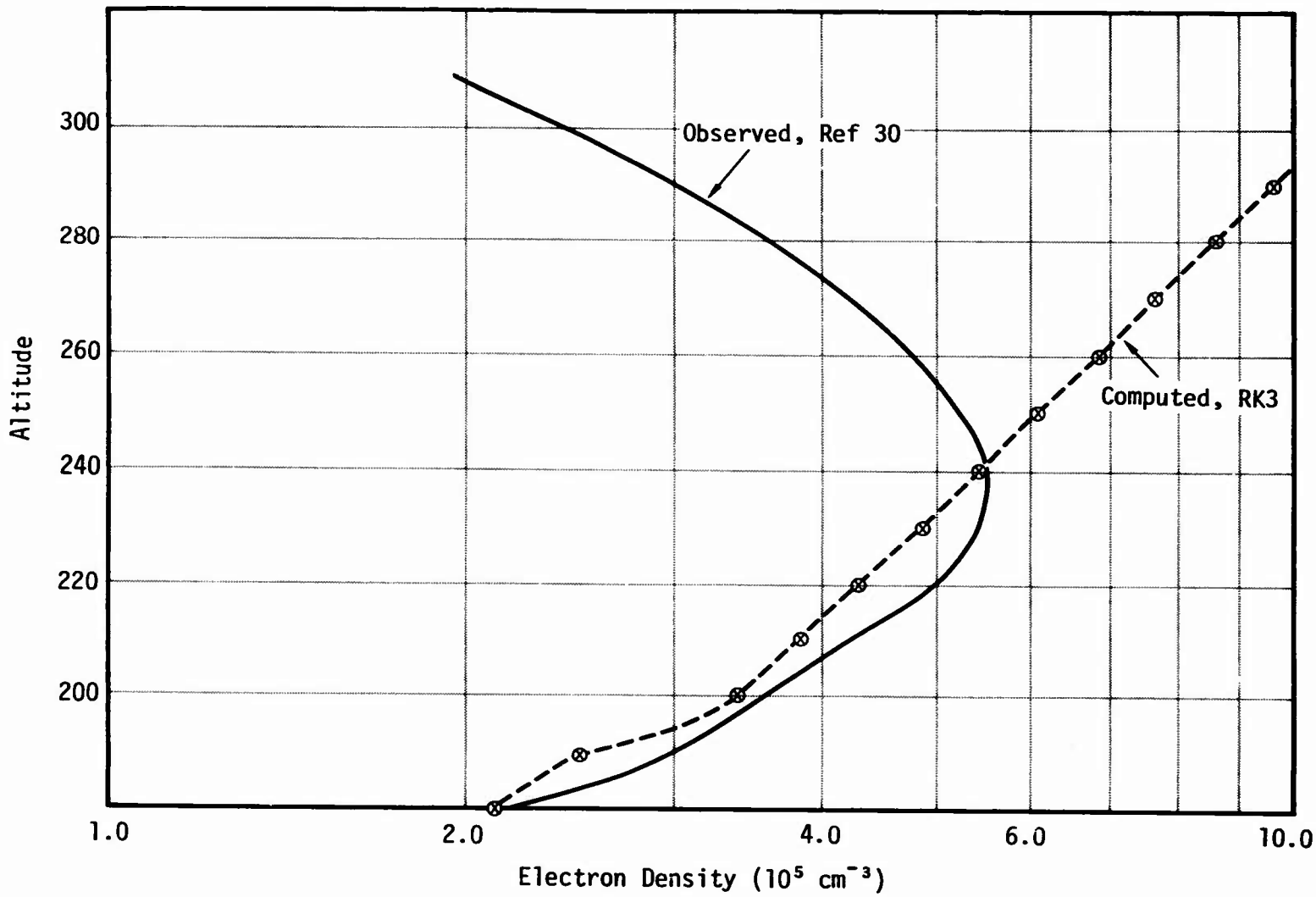

Figure 8. Comparison of Computed and Observed F_2-Region Electron Density Profiles.

magnetosphere and ionosphere is also important[4]. Walker and McElroy[34] estimate that transport terms can become comparable to chemical production and loss terms at 220 km and above during the day.

Despite the neglect of diffusion in our codes, the agreement between theory and experiment is satisfactory up to the F_2 peak.

SECTION 5

CONCLUSIONS

The addition of solar photoionization processes to existing chemistry codes developed for severely disturbed atmospheres associated with nuclear bursts can provide reasonably realistic daytime electron density profiles for quiet ambient conditions over an altitude range of 60-250 km (up to the F_2 peak). Some provisions for transport effects above 200 km is probably necessary in order to correctly compute electron density profiles above 250 km.

Nighttime ambient electron density profiles for the E and F_1 regions are less accurately predicted than daytime profiles and this may reflect the neglect of ion transport in the existing codes. Both the origin and intensity of natural nighttime ionization sources are uncertain and this must also be considered as a contributing factor.

The simplified but much faster SDCCHEM code can compute satisfactory E and F region ambient electron densities. This is encouraging in terms of using the program for late-time and large distance decoupled chemistry calculations in conjunction with phenomenology codes like MICE where computer running time considerations are important.

The computation of electron and ion density in ambient and very-slightly-perturbed atmospheres is but one of many aspects of the overall problem of nuclear effects on communication systems. Other aspects of the problem, such as calculation of atmospheric motion and fission debris position

over very large regions and for very long times, and the effect of the perturbed environment on transmission of information, are being studied under other contracts. Our goal is to be able to make reliable predictions of communication system performance in a nuclear environment. We are unable to say at this time what accuracy in the chemistry calculations wi'l ultimately be required to meet this goal. However, our impression from work reported here is that the chemical aspects of the problem are for the moment at least, relatively well-understood. Less well-in-hand are the fluid motion (transport) aspects of the problem, and the techniques by which the fluid motion and chemistry are tied together.

REFERENCES

1. R. E. Bourdreau, A. C. Aiken and J. L. Donley, J. Geophys. Res. 71, 727 (1966).

2. L. A. Hall and H. E. Hinteregger, J. Geophys. Res. 75, 6959 (1970).

3. CIRA 1965, North Holland, Amsterdam, 1965.

4. P. M. Banks and G. Kockarts, Aeronomy, Vols. 1 and 2, Academic Press, New York, 1973.

5. DNA Reaction Rate Handbook, 2nd Ed., DNA 1948H, Nov. 1972.

6. A. W. Ali and P. C. Kepple, "Solar Ionization Rates for the Ionospheric E, F, and D Regions", NRL Report 7598, Oct. 1973.

7. R. D. Hake, E. T. Pierce and W. Viezee, "Stratospheric Electricity", Final Report, SRI Project 1724, Apr. 1973.

8. W. Swider, J. Geophys. Res. 70, 4859 (1965).

9. T. Ogawa and T. Tohmatsu, J. Geophys. Res. 76, 6139 (1971).

10. T. Tohmatsu, J. Geophys. Res. 76, 6139 (1971).

11. T. J. Keneshea, R. S. Narcisi and W. Swider, J. Geophys. Res. 75, 845 (1970).

12. R. J. Francey, J. Geophys. Res. 75, 4849 (1970).

13. T. A. Potemra and A. J. Zmuda, J. Geophys. Res. 75, 7161 (1970).

14. D. H. Archer and P. W. Tarr, "Stimulated Skyglow", Final Tech. Report, RADC-TR-14-109, Jan. 1974.

15. M. Scheibe, "An Analytic Model for Nuclear Induced D-Region Chemistry", DNA 2920F, Oct. 1972.

REFERENCES (CONTINUED)

17. D. F. Strobel, J. Geophys. Res. 76, 2441 (1971).

18. A. P. Mitra and D. K. Chakrabarty, Space Res. 11, 1013 (1971).

19. E. A. Mechtly and S. A. Bowhill, J. Atmos. Terr. Phys. 34, 1899 (1972).

20. M. Scheibe, private communication.

21. R. P. Turco, "A Calculation of Photodissociation Rates in the Atmosphere Below 100 km", RDA Report RDA-TR-076-DNA, Apr. 1973.

22. F. D. Colgrave, F. S. Johnson and W. B. Hanson, J. Geophys. Res. 71, 222 (1966).

23. D. F. Strobel, D. M. Hunten and M. B. McElroy, J. Geophys. Res. 75, 4307 (1970).

24. M. A. Geller in "Cospar Symposium on D- and E-Region Ion Chemistry", Aeronomy Report No. 48, p. 88, Univ. of Illinois, Urbana, June 1972.

25. T. M. Donahue in "Cospar Symposium on D- and E-Region Ion Chemistry", Aeronomy Report No. 48, p. 136, Univ. of Illinois, Urbana, June 1972.

26. R. A. Goldberg in "Cospar Symposium on D- and E-Region Ion Chemistry", Aeronomy Report No. 48, p. 160, Univ. of Illinois, Urbana, June 1972.

27. R. S. Narcisi in "Cospar Symposium on D- and E-Region Ion Chemistry", Aeronomy Report No. 48, p. 221, Univ. of Illinois, Urbana, June 1972.

28. K. Maeda, Space Res. 12, 1229 (1972).

29. W. J. Heikkila, et al., J. Geophys. Res. 73, 3511 (1968).

30. C. Y. Johnson, J. Geophys. Res. 71, 330 (1966).

31. N. Wakai, J. Geophys. Res. 72, 4507 (1967).

32. J. C. Holmes, C. Y. Johnson and J. M. Young, Space Res. 5, 756 (1965).

33. R. D. Harris and T. Tomatsu in "Cospar Symposium on D- and E-Region Ion Chemistry", Aeronomy Report No. 48, p. 199, Univ. of Illinois, Urbana, June 1972.

34. J. C. G. Walker and M. B. McElroy, J. Geophys. Res. 71, 3779 (1966).

REFERENCES (CONTINUED)

35. T. R. Young and J. P. Boris,"A Numerical Technique for Solving Stiff Ordinary Differential Equations Associated with Reactive Flow Problems", NRL Mem. Report 2611, July 1973.

36. A. C. Hindmarsh, "Linear Multistep Methods for Ordinary Differential Equations: Method Formulations, Stability, and Methods of Nordseick and Gear", UCRL-51186, March 1972.

37. D. S. Sappenfield, "Radiation From a Recombining Oxygen Plasma", LASL Report LA-4303 Suppl., Feb. 1971.

APPENDIX A

E AND F REGION RK3 CODE

RK3 contains nearly 50 reactions involving 15 species. Table A-1 lists the reactions and rate constants included in RK3. The species followed are: N_2, O_2, NO, NO_2, O_3, O, $N(^4S)$, $N(^2D)$, N^+, $O^+(^4S)$, $O^+(^2D)$, NO^+, N_2^+, O_2^+ and excited $N_2(1)$. At present the N_2 vibrational temperature is taken to be the same as the gas kinetic temperature.

Any or all of the initial species densities may be specified at the start of a run. The total mass density and energy are also expected as input. Provision for conservation of species is in the code and was used in all the calculations done here.

The numerical integration of the 15 coupled rate equations is carried out by either one or both of two different methods, depending on the stiffness of the equations. The first method is relatively fast and works well for non-stiff to moderately stiff equations. It is based on the procedures developed by Young and Boris[35]. The second and often slower scheme carries out the integration by the Gear method[36]. It is used whenever the Young-Boris procedure time step fell below some critical value due to severe stiffness. For ambient conditions the Gear method is almost never necessary. This is, however, not true for severely disturbed atmospheres.

Table A-1. Reactions and Rate Constants in RK3*

	REACTION	a	b	c
1)	$N_2 + O \rightarrow NO + N(^4S)$	1.0(-10)	0	37900
2)	$N_2 + O^+(^4S) \rightarrow NO^+ + N(^4S)$**	2.24(-21)	2.75	-1390
3)	$N_2 + O^+(^2D) \rightarrow N_2^+ + O$	3.0(-10)	0	0
4)	$N_2 + N^+ \rightarrow N_2^+ + N(^4S)$	4.0(-11)	0	20600
5)	$N_2 + M \rightarrow N_2(1) + M$	9.97(-31)	4.478	7300
6)	$N_2 + e \rightarrow N_2(1) + e$	3.2(-16)	1.5	3480
7)	$O_2 + N(^4S) \rightarrow NO + O$	2.4(-11)	0	4000
8)	$O_2 + N(^2D) \rightarrow NO + O$	4.0(-13)	0.5	0
9)	$O_2 + O^+(^4S) \rightarrow O_2^+ + O$	3.4(-10)	-0.5	0
10)	$O_2 + O^+(^2D) \rightarrow O_2^+ + O$	3.0(-10)	0	0
11)	$O_2 + N^+ \rightarrow O_2^+ + N(^4S)$	2.0(-10)	0	0
12)	$O_2 + N^+ \rightarrow O_2^+ + N(^2D)$	1.0(-10)	0	0
13)	$O_2 + O + M \rightarrow O_3 + M$	6.8(-28)	-2.6	0
14)	$O_2 + N^+ \rightarrow NO^+ + O$	3.0(-10)	0	0
15)	$N(^4S) + NO + 5N_2 \rightarrow O + 6N_2(1)$	2.2(-11)	0	0
16)	$N(^4S) + O \rightarrow NO^+ + e$	1.8(-12)	0	31800
17)	$N(^4S) + e \rightarrow N(^2D) + e$	1.2(-9)	0	27700
18)	$N(^4S) + M \rightarrow N(^2D) + M$	7.5(-15)	0	27700
19)	$N(^4S) + O_3 \rightarrow NO + O_2$	2.0(-12)	0.5	1200
20)	$N(^2D) + NO + 9N_2 \rightarrow O + 10N_2(1)$	2.2(-11)	0	0
21)	$N(^2D) + O \rightarrow NO^+ + e$	1.8(-12)	0	4300
22)	$N(^2D) + e \rightarrow N(^4S) + e$	5.0(-10)	0	0
23)	$N(^2D) + M \rightarrow N(^4S) + M$	3.3(-15)	0	0
24)	$N(^2D) + NO \rightarrow N(^4S) + NO$	1.8(-10)	0	0

* The rate constants in this table are given in the form $k=aT^b e^{-c/T}$. In the a column read 1.0(-10) as 1.0×10^{-10}.

** This rate constant is limited to values of k for which $1.3(-12) < k < 1.0(-10)$

Table A-1 (Continued). Reactions and Rate Constants in RK3.

	REACTION	a	b	c
25)	$O + O_3 \rightarrow 2O_2$	1.4(-11)	0	2200
26)	$O + NO + M \rightarrow NO_2 + M$	2.9(-33)	0	940
27)	$O + NO \rightarrow NO_2 + h\nu$	4.1(-12)	-1.94	0
28)	$O + NO_2 \rightarrow NO + O_2$	1.6(-11)	0	300
29)	$O + NO \rightarrow O_2 + N(^4S)$	5.3(-12)	0	20200
30)	$N^+ + NO \rightarrow NO^+ + N(^4S)$	4.0(-10)	0	0
31)	$N^+ + NO \rightarrow NO^+ + N(^2D)$	4.0(-10)	0	0
32)	$N^+ + e \rightarrow N(^4S) + h\nu$	(As in Reference 37)		
33)	$O^+(^4S) + e \rightarrow O^+(^2D) + e$	2.5(-8)	0	38504
34)	$O^+(^4S) + M \rightarrow O^+(^2D) + M$	1.0(-12)	0	28504
35)	$O^+(^4S) + e \rightarrow O + h\nu$	(As in Reference 37)		
36)	$O^+(^2D) + e \rightarrow O^+(^4S) + e$	1.0(-8)	0	0
37)	$O^+(^2D) + M \rightarrow O^+(^4S) + M$	1.0(-12)	0	0
38)	$O^+(^2D) + e \rightarrow O + h\nu$	(As in Reference 37)		
39)	$NO^+ + e \rightarrow \frac{1}{4} N(^4S) + \frac{3}{4} N(^2D) + O$	6.9(-6)	-0.5	0
40)	$NO + O_3 \rightarrow NO_2 + O_2$	9.5(-13)	0	1300
41)	$O_3 + h\nu \rightarrow O_2 + O$	1.0(-2)	0	0
42)	$N_2^+ + e \rightarrow N(^4S) + N(^2D)$	8.3(-7)	-0.2	0
43)	$N_2^+ + O_2 \rightarrow O_2^+ + N_2$	8.5(-10)	-0.5	0
44)	$N_2^+ + NO \rightarrow NO^+ + N_2$	3.3(-10)	0	0
45)	$N_2^+ + O \rightarrow \frac{1}{2} N(^4S) + \frac{1}{2} N(^2D) + NO$	6.0(-10)	0	0
46)	$O_2^+ + e \rightarrow 2O$	1.1(-5)	-0.7	0
47)	$O_2^+ + NO \rightarrow O_2 + NO^+$	6.3(-10)	0	0
48)	$N_2(1) + M \rightarrow N_2 + M$	9.97(-31)	4.748	3876
49)	$N_2(1) + e \rightarrow N_2 + e$	3.20(-16)	1.5	0

INSERT TO

DNA 3520T dated 14 February 1975

The following reference relates to this document and has distribution limited to U.S. Government agencies only. This list is provided to all addressees on initial distribution except DDC/NTIS.

1. Sappenfield, D.S. and Fajen, F.E. "Fireballs and Beta Streamers in the Kingfish-Teak Altitude Regime (U)," DNA 3189F, December 1973 (SECRET, RESTRICTED DATA).